Comput Mech (2009) 44:433–445
DOI 10.1007/s00466-009-0382-7

ORIGINAL PAPER

Multi-length scale micromorphic process zone model

Franck Vernerey · Wing Kam Liu · Brian Moran · Gregory Olson

Received: 7 January 2009 / Accepted: 9 February 2009 / Published online: 20 March 2009

Abstract The prediction of fracture toughness for hierarchical materials remains a challenging research issue because it involves different physical phenomena at multiple length scales. In this work, we propose a multiscale process zone model based on linear elastic fracture mechanics and a multiscale micromorphic theory. By computing the stress intensity factor in a K-dominant region while maintaining the mechanism of failure in the process zone, this model allows the evaluation of the fracture toughness of hierarchical materials as a function of their microstructural properties. After introducing a multi-length scale finite element formulation, an application is presented for high strength alloys, whose microstructure typically contains two populations of particles at different length scales. For this material, the design parameters comprise of the strength of the matrix–particle interface, the particle volume fraction and the strain-hardening of the matrix. Using the proposed framework, trends in the fracture toughness are computed as a function of design parameters, showing potential applications in computational materials design.

Keywords Multiscale micromorphic theory · Fracture mechanics · Materials design · Ductile failure · Multi-length scale finite elements

F. Vernerey (✉)
Department of Civil, Environmental and Architectural Engineering, University of Colorado at Boulder, Campus Box 428, Boulder, CO 80309-0428, USA
e-mail: franck.vernerey@colorado.edu; vernerey@colorado.edu

W. K. Liu (✉)
Department of Mechanical Engineering, Northwestern University, 2145 Sheridan Road, Evanston, IL 60208-3111, USA
e-mail: w-liu@northwestern.edu

B. Moran
Department of Civil Engineering, Northwestern University, 2145 Sheridan Road, Evanston, IL 60208-3111, USA

G. Olson
Department of Material Science and Engineering, Northwestern University, 2145 Sheridan Road, Evanston, IL 60208-3111, USA

1 Introduction

For the design of stronger and tougher materials, it is desirable to quantify the relationship between their fracture toughness and key microstructural parameters. While this relationship is generally too complicated to be determined through experiments, physically based theoretical and computational models seem to be the key to making quantitative predictions. A major difficulty in this approach is the disparity of microstructural length scales to be considered in the fracture of material, rendering computations either unaffordable or inaccurate. In this paper, we propose to tackle this issue with a new approach, the multiscale process zone model, which encompasses the following features:

- The model is applicable to a large class of hierarchical materials and accounts for size effects associated with various level of microstructure.
- The approach leads to affordable computations and does not require an explicit modeling of the microstructure in the region of the crack tip.
- The model permits the computation of fracture toughness as a function of key microstructural parameters. This is an important feature for the applicability of the method to material design.

The multiscale model is illustrated with the computation of the fracture properties of high strength alloys (HSA), whose microstructure consists of population of inclusions at two distinct length scales, embedded in a metallic matrix. The study of the fracture of those materials has been an active field of research for decades and many aspects of its underlying mechanisms have been addressed in the literature [2,6,7,9,10,12,17–21,27,30]. In particular, those studies identified the mechanism of ductile fracture as nucleation, growth and coalescence of voids around inclusions. The first attempt to include the effect of porosity on the growth of ductile crack was made by Rice and Johnson [26] who predicted that fracture toughness should depend on the characteristic spacing and size of inclusions. Recently, efforts on modeling ductile crack growth made use of numerical models. As pointed out by Pardoen and Hutchinson [24], there are mainly three types of analyses.

The first category involves the modeling of crack growth with a cohesive model [28,29]. In this approach, the crack is viewed as the boundary between two separate bodies, which are bonded by a traction-separation relation. This relation has the advantage of possessing a length scale that can be connected to the size of the microstructure. However, the approach suffers from several drawbacks. First, cohesive zone models are known to suffer from difficulties with respect to ductile fracture in properly scaling effects of plastic dissipation away from the cohesive surface. Second, the area under the force-separation curve represents the energy of separation, which is closely related to the concept of fracture toughness. However, this approach is empirical and thus, the connection between the traction–separation relation and failure mechanisms is ambiguous in front of a crack tip. This constitutes a major concern in materials design.

In order to establish a direct relation between the physics of crack growth and the fracture toughness, a second approach is the explicit modeling of the material's microstructure in the crack tip region using the finite element method. Using this approach, Aravas and McMeeking [1] studied the effects of a statistical distribution of voids in HSA on crack growth. The method also permitted the characterization of the effect of voids present at two different length scales by modeling large voids in a homogenized porous matrix [5,22]. However, as the full details of the microstructure must be represented, this method is computationally intense and therefore not practical for parametric studies. Modeling microstructural damage often involves extremely large deformation, which may cause a convergence issue with the finite element method. To address this issue, meshfree particle methods [11,13,14] have been developed, which avoided remeshing of the entire domain due to element distortion.

Finally, the third category of models uses homogenized constitutive relations to account for void growth and coalescence [15]. The strength of these models is that they offer great flexibility in tuning material parameters such as void volume fraction, yield stress or nucleation strain, and this makes them good candidates for materials design. However, for local models (size independent), the microstructural length scale is not represented, consequently, limiting their applications for when the size of the microstructure plays a significant role. Nonlocal models in the context of fracture mechanics have been investigated by Yan and Mai [37], Xia et al. [33–36] as well as Chen [4] and Huang [8] but these studies were limited to hardening, strain gradient plasticity. Needleman and Tvergaard [23] investigated ductile crack growth using a nonlocal damage model. This work predicted a rise in the material's resistance to crack propagation as the size of the microstructure is increased. However, this approach is limited to material possessing only one microstructural length scale.

The present work introduces a multiscale continuum formulation that provides an alternative to the above techniques. The paper is organized as follows. In Sect. 2, we start by discussing the assumptions and layout of the multiscale process zone model. In Sect. 3, we then describe the multiscale model and its multi-length scale finite element model for the failure of HSA, followed by the investigation of the fracture toughness as a function of some key nano-, micro-, and macro-design parameters. The variation of fracture toughness with various microstructural details is then investigated in Sect. 4. To conclude, Sect. 5 gives a short summary of the work and discusses future research directions.

2 Multiscale process zone model

One of the main issues in the study of materials fracture resides in the fact that *both large scale features and small features must be considered concurrently*. This is due to the fact that the computation of *fracture toughness is performed on a macroscopic specimen while the mechanisms of fracture typically occur at the micro/nano scales*. We tackle this issue by proposing a multiscale process zone model based on a fusion of two approaches: linear elastic fracture mechanics (LEFM) and the multiscale micromorphic theory [31,32]. For the design of HSA, it is of interest to qualitatively understand how fracture toughness varies with some key microstructural parameters. Understanding these trends, together with optimization techniques, will eventually permit the determination of a microstructure of HSA that lead to maximal strength and toughness, hence providing a stepping-stone for computational material design.

2.1 The structure of HSA

The microstructure of HSA consists of a metallic matrix in which two populations of particles are found at distinct

Table 1 Material constants of HSA for steel matrix, TiN and TiC particles

σ_y (GPa)	1.7
h (GPa)	0.6
σ^p (GPa)	1.0
σ^s (GPa)	4.1
f^p	0.01
f^s	0.02

scales. On the one hand, the desirable population of secondary particles (TiC) is found in the range of 10–100 nm and has the effect of increasing the strength of an alloy matrix (in this example, the matrix material is steel). On the other hand, the primary particles (TiN), a byproduct of the manufacture process, are found in the range of microns and are known to decrease fracture toughness. At each scale, the size of particles, their bonding strength with the matrix material and the properties of the matrix material are quantities that can be controlled during the manufacturing process and can therefore be considered as design parameters. The mean values of the yield stress σ_y, the hardening parameter h of the matrix, the debonding stresses σ^p (primary particles) and σ^s (secondary particles) at the particle/matrix interface and the particle volume fractions f^p (primary particles) and f^s (secondary particles) of the material investigated in this study are reported in Table 1.

2.2 Multi-length scale process zone framework

Consider the specimen with a pre-existing crack depicted on the left of Fig. 1. In a region near the crack tip, LEFM tells us that the dominant stress field varies as $r^{-1/2}$ (where r is the distance from the crack tip) and is quantified by the stress intensity factor K. This region of validity of LEFM (the K-dominant region) is bounded at both small and large scales as follows:

- At scales that are small compared to the size of the specimen, the LEFM equations are valid in a region that is far enough from the crack tip neighborhood in which stresses deviate from linearity. This is called the small scale yielding assumption [25].
- At large scales, the stress field is governed by the geometry of the specimen and diverges from the K-field.

In the region of the crack tip, crack growth can generally be attributed to localized material failure at the microstructural scales whose mechanisms are depicted in the schematics in Fig. 1 for HSA. To summarize, the failure of HSA in front of a pre-existing crack tip is attributed to the nucleation, growth and coalescence of voids nucleating from inclusions (represented by square and circular shapes). In this study, we do not consider particle cracking, keeping in mind that this phenomenon can later be added to the model. Crack blunting is due to plastic deformation and void growth, while crack advance results from the coalescence and linking of neighboring voids in front of the crack tip. Localization may occur at two distinct length scales during this process; during the growth of larger voids (from primary inclusion), plastic strain typically localizes in a region dictated by the size of those voids (denoted as ℓ_1 in Fig. 1). After subsequent deformation, nucleation of smaller voids (called "microvoids"), occurs at the sites of secondary particles. At this point, the size of the localization region becomes comparable to the size of microvoids (denoted as ℓ_2 in Fig. 1). These microvoids grow rapidly to connect the crack tip and the larger void, resulting in crack advance.

These observations are the base for the micromorphic process zone model described in this paper. Let us consider a crack in a circular region Ω_{ssy} of diameter $2r_K$ centered at the crack tip (Fig 1) such that the boundary Γ_{ssy} of Ω_{ssy} is in the K-dominant region and the deformations are macroscopic. The contributions from microscopic fields therefore vanish and the stress intensity factor K_I is only related to the macroscopic displacement $\mathbf{u}$ on Γ_{ssy} by:

$$u_1 = \frac{K_I}{2\mu}\sqrt{\frac{r_K}{2\pi}}\cos\left(\frac{\theta}{2}\right)\left[\kappa - 1 + 2\sin^2\left(\frac{\theta}{2}\right)\right]$$
$$u_2 = \frac{K_I}{2\mu}\sqrt{\frac{r_K}{2\pi}}\sin\left(\frac{\theta}{2}\right)\left[\kappa + 1 - 2\cos^2\left(\frac{\theta}{2}\right)\right] \quad (1)$$

where θ is the angle between the x axis and a line passing through the crack tip and the point at which the displacement is computed. For plane strain, we have $\kappa = 3 - 4\mu$ where μ is the Poisson's ratio. Equation (1) provides displacement boundary conditions for the boundary value problem of a circular region loaded with a remote K-field.

Near the crack tip region, the heterogeneous deformation of the microstructure becomes important and thus, the conventional continuum approach based on the Cauchy stress $\boldsymbol{\sigma}$ and the rate of deformation $\mathbf{D}$ loses its validity. To overcome this issue, we present a multiscale micromorphic formulation [31] that permits the incorporation of the material's internal length scales through the strain gradient and stress couples. We show that this model is a good candidate for studying the fracture of hierarchical materials.

3 Multiscale continuum model for the failure of HSA

We now introduce the continuum formulation, numerical implementation and constitutive relation used to model the process zone region.

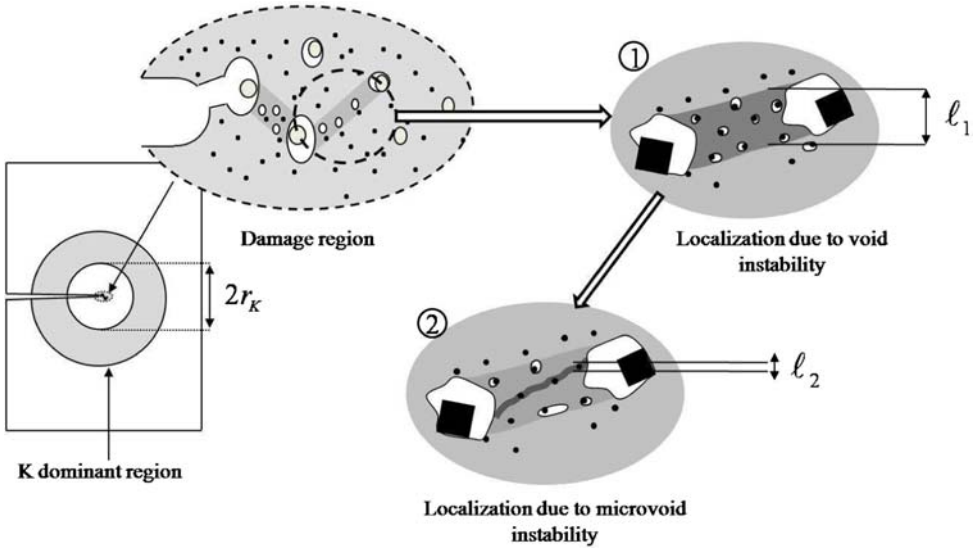

Fig. 1 K-dominant region and zone of microstructure damage in a fracture specimen. Process zone model showing the full computational domain for the multiscale process zone model and a zoom of the FEM description around the crack tip

3.1 Multiscale micromorphic model for HSA

Continuum formulations of the strain softening and localization in solids are known to be an issue since the conventional continuum theory does not possess a length-scale in this formulation. This usually leads to a localization region that is not defined, leading to an inadequate estimation of the material behavior after the onset of strain softening. Alternative strategies thus consist in introducing a length-scale into the continuum theory through the incorporation of a second displacement gradient into the expression of the internal energy of the solid. This concept led to micromorphic and strain gradient theories, which possess an intrinsic length scale characterizing the localization region. This paper is concerned with a hierarchical material (HSA), for which localization and failure occurs at several length-scales which can be modeled with the multiscale micromorphic framework developed by Vernerey et al. [30]. Next, we present the model for the failure of HSA, for which localization involves two characteristic length scales associated with the size of primary and secondary inclusions.

The multiscale model for the failure of HSA is based on the multiscale decomposition of the microstructure according to three averaging domains $\bar{\Omega}$, Ω^1 and Ω^2 that can be thought of as representative volume element for the entire microstructure, the material consisting of secondary particles only and the matrix material, respectively (Fig. 2). Based on this decomposition, we introduce three deformation measures as average velocity gradients into each domain: the macro-velocity gradient $\mathbf{L}$ (averaged in $\bar{\Omega}$), the micro-velocity $\mathbf{L}^1$ (averaged in Ω^1), and submicro-velocity gradient $\mathbf{L}^2$ (averaged in Ω^2). For further details regarding kinematics, the reader is referred to Vernerey et al. [30].

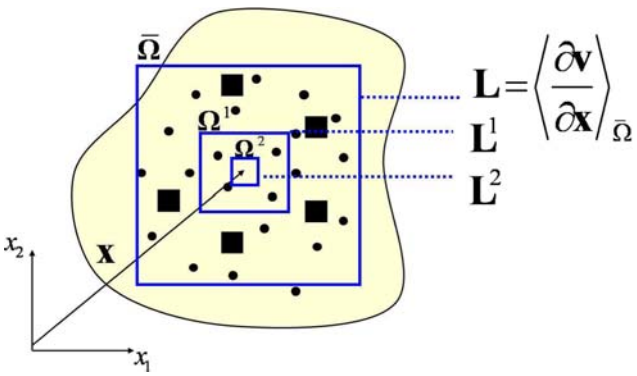

Fig. 2 Proposed multiscale framework for the modeling of HSA. The *squares* represent the primary particles and the *circles* represent the secondary particles

The expression of internal energy of the multiscale continuum can then be introduced. Only including the effect of stretches at microscale, the internal energy may be written in terms of the symmetric counterparts $\mathbf{D}^1$ and $\mathbf{D}^2$ of the micro-velocity gradients $\mathbf{L}^1$ and $\mathbf{L}^2$; this means that the variation of internal power δP_{int} can then be written in terms of the variation of the rates of deformation $\delta\mathbf{D}$, $\delta\mathbf{D}^1$, $\delta\mathbf{D}^2$ and their first gradients as follows:

$$\delta P_{\text{int}} = \int_{\Omega} \left\{ \boldsymbol{\sigma} : \delta\mathbf{D} + \bar{\boldsymbol{\beta}}^1 : \delta\left(\mathbf{D}^1 - \mathbf{D}\right) + \bar{\bar{\boldsymbol{\beta}}}^1 \vdots \delta\mathbf{D}^1 \overleftarrow{\nabla} + \bar{\boldsymbol{\beta}}^2 : \delta\left(\mathbf{D}^2 - \mathbf{D}\right) + \bar{\bar{\boldsymbol{\beta}}}^2 \vdots \delta\mathbf{D}^2 \overleftarrow{\nabla} \right\} d\Omega \tag{2}$$

where $\boldsymbol{\sigma}$ is the symmetric macro-stress (Cauchy stress), $\bar{\boldsymbol{\beta}}^1$ and $\bar{\bar{\boldsymbol{\beta}}}^1$ are the micro-stress and microsopic stress couples and

$\overline{\overline{\boldsymbol{\beta}}}^2$ and $\overline{\overline{\overline{\boldsymbol{\beta}}}}^2$ are the submicro-stress and submicroscopic stress couples. A physical interpretation of the various terms can be given as follows. The quantity $\mathbf{D}^1 - \mathbf{D}$ is the inhomogeneous deformation resulting from the localization that occurs from the nucleation of large voids (from primary particles), and the inhomogeneous deformation $\mathbf{D}^2 - \mathbf{D}$ is the result of the localization that occurs from nucleation of micro-voids (from secondary particles). The micro-stresses (submicro-stresses, respectively) are interpreted as the stresses and stress moments exerted by the microstructure to redistribute plastic deformation around large voids (micro-voids, respectively). It is important to notice that the stress couples have the dimension of a stress times a length, and are thus responsible for incorporating "size effects" into the model. In this particular model, the microstress couple $\overline{\overline{\boldsymbol{\beta}}}^1$ is associated with size effects at the scale of primary inclusions while the microstress couple $\overline{\overline{\overline{\boldsymbol{\beta}}}}^2$ is associated with size effects at the scale of secondary inclusions.

For a time-independent problem, the kinetic power vanishes and the external power can be written in terms of macroscopic body forces through the vector $\mathbf{b}$ and surface traction through $\mathbf{t}$ (we ignore microscopic double traction in this case). By using variational principles, one can show that the strong form of the governing equation is the following system of coupled differential equations and boundary conditions:

$$\begin{aligned}
&\left(\boldsymbol{\sigma} - \overline{\boldsymbol{\beta}}^1 - \overline{\boldsymbol{\beta}}^2\right) \cdot \overleftarrow{\nabla} = \mathbf{b} \quad \text{in } \Omega \\
&\left(\boldsymbol{\sigma} - \overline{\boldsymbol{\beta}}^1 - \overline{\boldsymbol{\beta}}^2\right) \cdot \mathbf{n} = \mathbf{t} \quad \text{on } \Gamma_t \\
&\overline{\overline{\boldsymbol{\beta}}}^1 \cdot \overleftarrow{\nabla} - \overline{\boldsymbol{\beta}}^1 = 0 \quad \text{in } \Omega, \qquad \overline{\overline{\boldsymbol{\beta}}}^1 \cdot \mathbf{n} = 0 \quad \text{on } \Gamma_t \\
&\overline{\overline{\overline{\boldsymbol{\beta}}}}^2 \cdot \overleftarrow{\nabla} - \overline{\overline{\boldsymbol{\beta}}}^2 = 0 \quad \text{in } \Omega, \qquad \overline{\overline{\overline{\boldsymbol{\beta}}}}^2 \cdot \mathbf{n} = 0 \quad \text{on } \Gamma_t
\end{aligned} \tag{3}$$

While the first equation represents the general equilibrium of a material point, the second and third equations are the equilibrium of the stresses and stress couples arising at the micro and submicro-scale.

3.2 A multi-length scale finite element method

A multi-length scale finite element framework is now introduced to solve the system of Eqs. (3). In order to remain in the classical element formulation, we first generalize the stress and strain measures such that when micro and submicro stresses are present, the conventional stress and strain measures are replaced by the generalized stress vectors $\boldsymbol{\Sigma}$ and $\boldsymbol{\Delta}$:

$$\begin{cases}
\boldsymbol{\Sigma} = \left[\begin{array}{ccccc} \boldsymbol{\sigma} & \overline{\boldsymbol{\beta}}^1 & \overline{\overline{\boldsymbol{\beta}}}^1 & \overline{\boldsymbol{\beta}}^2 & \overline{\overline{\overline{\boldsymbol{\beta}}}}^2 \end{array}\right] \\
\boldsymbol{\Delta} = \left[\begin{array}{cccc} \mathbf{D} & \left[\mathbf{D}^1 - \mathbf{D}\right] & \mathbf{D}^1 \overleftarrow{\nabla} & \left[\mathbf{D}^2 - \mathbf{D}\right] & \mathbf{D}^2 \overleftarrow{\nabla} \end{array}\right]
\end{cases} \tag{4}$$

where the stresses $\boldsymbol{\sigma}$, $\overline{\boldsymbol{\beta}}^I$, and $\overline{\overline{\boldsymbol{\beta}}}^I$ and the corresponding strains are in the form of three, 3- and 6-dimensional vectors (for a 2-dimensional problem), respectively. Using this notation, it is straightforward to show that the variation of internal power (2) can be written in a more conventional form:

$$\delta P_{\text{int}} = \int_{\Omega} \boldsymbol{\Sigma} \cdot \delta \boldsymbol{\Delta} d\Omega \tag{5}$$

The finite element formulation thus follows from discretizing the domain of analysis with elements and nodes and introducing the degrees of freedom at each node α with the vector $\mathbf{d}_\alpha$:

$$\mathbf{d}_\alpha \equiv \begin{bmatrix} \mathbf{v}_\alpha \\ \mathbf{D}^1_\alpha \\ \mathbf{D}^2_\alpha \end{bmatrix} \tag{6}$$

where $\mathbf{v}_\alpha$, $\mathbf{D}^1_\alpha$ and $\mathbf{D}^2_\alpha$ are the nodal velocity and rates of microdeformation, respectively. Let $\mathbf{d}^e$ be the assembly of all of the $\mathbf{d}_\alpha$ in an element. We now introduce the matrix $\mathbf{N}^e$ of shape functions (which only need to contains C^0 functions) such that the velocity and rates of micro-deformation are written as an interpolation of the nodal degrees of freedom as follows:

$$\begin{bmatrix} \mathbf{v}(\mathbf{x}) \\ \mathbf{D}^1(\mathbf{x}) \\ \mathbf{D}^2(\mathbf{x}) \end{bmatrix} = \mathbf{N}^e(\mathbf{x})\, \mathbf{d}^e \tag{7}$$

Similarly, a matrix $\mathbf{Q}^e$ containing spatial derivatives of shape functions can be introduced, such that the generalized strain rate within the element is written:

$$\boldsymbol{\Delta}(\mathbf{x}) = \mathbf{Q}^e(\mathbf{x})\, \mathbf{d}^e \tag{8}$$

Using these definitions, the discretized form of the variation of internal power (2) can simply be written:

$$\delta P_{\text{int}} = \sum_{e=1}^{n_e} \left\{ \int_{\Omega_e} \left(\delta \mathbf{d}^e\right)^T \mathbf{Q}^T \boldsymbol{\Sigma} d\Omega_e \right\} = \left(\delta \mathbf{d}^e\right)^T \mathbf{f}^{\text{int}} \tag{9}$$

where the number of elements is given by n_e, the internal force by the vector $\mathbf{f}^{\text{int}}$. Defining $\mathbf{L}_e$ as the connectivity matrix of the system, we have:

$$\mathbf{f}^{\text{int}} = \sum_{e=1}^{n_e} \mathbf{L}_e^T \left\{ \int_{\Omega_e} \mathbf{Q}^T \boldsymbol{\Sigma} d\Omega_e \right\} \tag{10}$$

Similarly, we can obtain a vector of external forces $\mathbf{f}^{\text{ext}}$ such that the discrete equation of motion is written in a similar form as the standard finite element method:

$$\mathbf{f}^{\text{int}} = \mathbf{f}^{\text{ext}} \tag{11}$$

In this work, the above equation is solved with an explicit scheme, such as that addressed in Vernerey et al. [30]. The solution is computed with an explicit dynamic scheme in quasi-static conditions. This is ensured by enforcing a very slow loading rate compared to the speed of elastic waves. The implementation of the nonlinear constitutive relation follows from a semi-implicit backward Euler scheme introduced in Belytschko et al. [3].

3.3 A multiscale damage model for HSA

As depicted in Fig. 1, the failure of HSA is characterized by three stages following the onset of softening. The first stage is dominated by the material instability associated with the nucleation and growth of voids around primary inclusions. The characteristic size ℓ_1 of these voids dictates the size of the localization region. The second stage is caused by the nucleation and growth of microvoids from secondary particles. This causes the size of localization region to reduce to the characteristic size ℓ_2 of microvoids. Finally, fracture occurs due to the rupture of the ligament between microvoids. The transition between each stage can be viewed as the onset of material instabilities occurring at different length-scales of the material's microstructure. From a modeling viewpoint, each instability can be represented by a yield criterion. This means that the failure of HSA can be characterized by three yield criteria associated with localization around larger voids, localization around micro-voids and finally, final fracture. This idea is illustrated in Fig. 3 showing the evolution of equivalent measures of the macro-stress σ, micro-stress β^1 and submicro-stress β^2. These measures are scalar quantities measuring the magnitude of $\boldsymbol{\sigma}$, a combination of $\overline{\boldsymbol{\beta}}^1$ and $\overline{\overline{\boldsymbol{\beta}}}^1$ and a combination of $\overline{\boldsymbol{\beta}}^2$ and $\overline{\overline{\boldsymbol{\beta}}}^2$, respectively. They are defined as follows:

$$\sigma = \sqrt{\frac{3}{2}\boldsymbol{\sigma}^{\mathrm{dev}} : \boldsymbol{\sigma}^{\mathrm{dev}}} \quad \text{and} \qquad \beta^{\alpha} = \sqrt{\frac{3}{2}\overline{\boldsymbol{\beta}}^{\alpha,\mathrm{dev}} : \overline{\boldsymbol{\beta}}^{\alpha,\mathrm{dev}} + \left(\frac{18}{\ell^1}\right)^2 \overline{\overline{\boldsymbol{\beta}}}^{\alpha,\mathrm{dev}} \cdot \overline{\overline{\boldsymbol{\beta}}}^{\alpha,\mathrm{dev}}} \tag{12}$$

The first instability corresponds to the onset of softening of the macro-stress and results in a localization of the deformation in a region dictated by the microstresses $\overline{\boldsymbol{\beta}}^1$ and $\overline{\overline{\boldsymbol{\beta}}}^1$ (associated with primary inclusions). The second instability corresponds to the onset of microstress (β^1) softening. This means that the size effect associated with ℓ_1 disappears and the size effect associated with ℓ_2 appears. Typically, the deformation will localize in a region (whose size is comparable to ℓ_2) dictated by the submicro-stresses $\overline{\boldsymbol{\beta}}^2$ and $\overline{\overline{\boldsymbol{\beta}}}^2$. The last instability corresponds to the onset of softening of the stress β^2. In other words, all effects of size are lost and final fracture is reached.

In a constitutive relation, instabilities are modeled with three yield functions (or plastic potentials in the context of associative plasticity): the macro-potential $\Phi(\boldsymbol{\sigma})$ and the first and second micro-potential $\Phi^1(\overline{\boldsymbol{\beta}}^1, \overline{\overline{\boldsymbol{\beta}}}^1)$ and $\Phi^2(\overline{\boldsymbol{\beta}}^2, \overline{\overline{\boldsymbol{\beta}}}^2)$, respectively. The macroscopic yield function Φ describes the

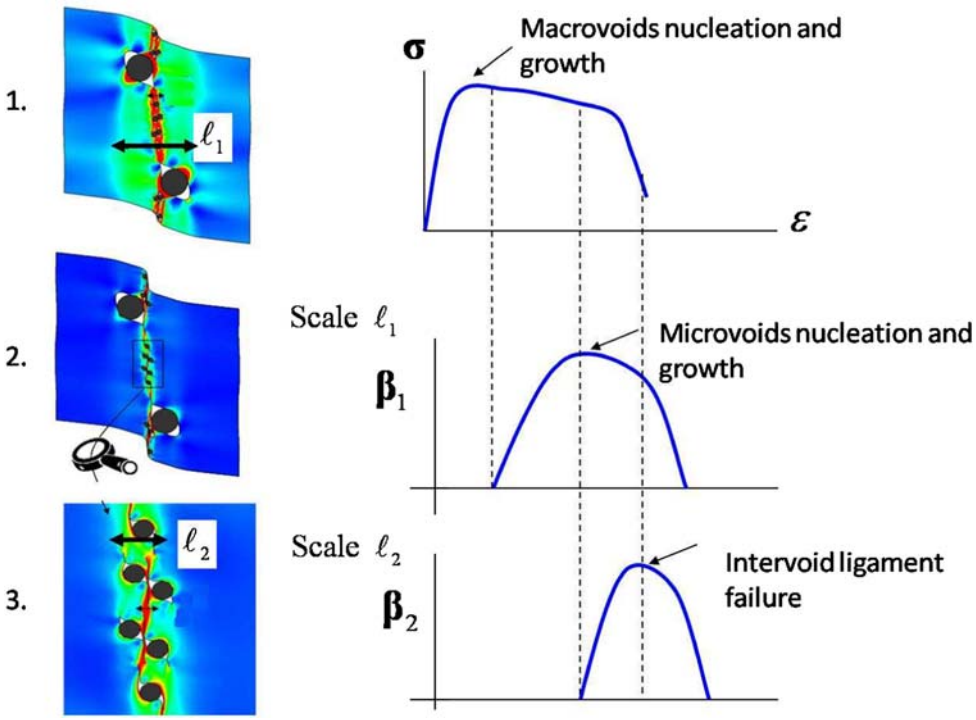

Fig. 3 Illustration of the constitutive relation governing the failure of HSA

evolution of the macro-stress and plastic strains and therefore represents the macroscopic plastic flow derived within the hierarchical methodology. The constitutive relation at the macro-scale:

$$\Phi(\boldsymbol{\sigma}) = \left(\frac{\sigma_{\text{eq}}}{\sigma_y}\right)^2 - 1 + 2q_1\left(f^P + f^S\right) \times \cosh\left(\frac{3q_2\sigma_m}{2\sigma_y}\right) - q_3\left(f^P + f^S\right)^2 = 0, \quad (13)$$

has the form of a GTN model [6,22] where f^P is the porosity nucleating from primary particles, f^S is the porosity due to the nucleation of voids from secondary particles and ε, σ_{eq} and σ_m are the effective plastic strain, the equivalent stress and the hydrostatic stress, respectively. While this function was initially derived based on void growth in an incompressible, perfectly plastic medium, and then modified for nucleation and coalescence effects, we assume that the general form holds for a hardening material. A detailed study of the extension of the GTN model is provided in McVeigh et al. [20]. Generally, this function accounts for the loss of load carrying capacity of the material due to the cumulative effects of void nucleation, growth and coalescence from both the primary and secondary particles.

The micro-stresses $(\overline{\boldsymbol{\beta}}^1, \overline{\overline{\boldsymbol{\beta}}}^1)$ are the local stress and moment generated in the material by larger voids as they grow. When the matrix material fails, the micro-couple and micro-stress can no longer be sustained to the same extent, that is, they yield. The yielding point of the micro-stress is controlled by the degradation and strain localization in the material between the primary particles, which is driven by the formation of a void sheet mechanism originating at the scale of the secondary particles. The microscopic plastic deformation is therefore a function of the nucleation and growth of secondary particle nucleated voids (void sheet). As such, volumetric deformation must be accounted for. A simple model can be developed in the form of a Drucker–Prager plasticity model, modified to account for the effects of higher order stress. It is written in the form:

$$\Phi^1\left(\overline{\boldsymbol{\beta}}^1, \overline{\overline{\boldsymbol{\beta}}}^1\right) = \left(\beta^1 + \alpha\beta_m^1\right) - \beta_y^1 = 0 \quad (14)$$

where β^1 and β_m^1 are the equivalent and the hydrostatic micro-stresses that are modified to account for the effects of higher order stress. The quantity β_y^1 is the microscopic yield stress that is a function of the microscopic effective plastic strain E^1.

Finally, the inhomogeneous stress distribution around voids (nucleated from the secondary particle) is provided by the submicro-stress and submicro-stress couples. At this scale, the stresses yield when the matrix material loses its capacity to transmit stresses; this occurs when the ligament between adjacent voids becomes unstable. Submicroscopic plastic deformation is therefore interpreted as plastic flow in the matrix material after the onset of void coalescence. The matrix behavior is assumed to be that of an incompressible plastic continuum; the plastic potential is thus taken in the form of J_2 flow plasticity modified to account for the effects of the stress couple:

$$\Phi^2\left(\overline{\boldsymbol{\beta}}^2, \overline{\overline{\boldsymbol{\beta}}}^2\right) = \beta^2 - \beta_y^2 = 0 \quad (15)$$

where β^2 and β_y^2 are the overall equivalent micro-stress and the submicro-yield stress respectively. The stress β_y^2 is a function of the sub-microscopic effective plastic strain E^2. A detailed description of the above plasticity model is given in Vernerey et al. [31].

3.4 Determination of material constants from homogenization

An important application of the presented multiscale model is the prediction of material properties and their relation to design parameters, emphasizing on fracture. Design parameters include inclusion size and distribution, matrix/particle interface properties, as well as the properties of the matrix material, such as yield strength and strain hardening parameter. In the present model, the relation between constitutive law and design parameters is accomplished by using computational homogenization, a procedure that consists in defining a representative volume of the microstructure, modeling its deformation with the finite element method, and extracting the relationship between the average constitutive relation and microstructural features. Such an analysis has been described in Vernerey et al. [31,32].

In this paper, we describe the determination of onset of void initiation, an important player in the fracture of alloys. When dealing with fracture, it is critical to quantify the level of macroscopic plastic strain at the onset of voids nucleation from particles (denoted by the "nucleation plastic strain"). In particular, it is of interest to understand how this parameter depends on the debonding peak stress at the matrix/particle interface and the strain hardening parameters of the matrix material. For this, computational cell models are carried out for the nucleation strain of primary particles; results are presented in Fig. 4. The idea consists on modeling the microstructure within a representative domain with the finite element method, applying an average deformation and relating the average properties (such as average plastic strain at nucleation) to local properties (such as debonding stress and strain hardening parameter). In the present work, the behavior of particle/matrix interface was modeled with a cohesive formulation (presented in McVeigh et al. [20]), for which the traction-separation behavior is depicted in Fig. 4. The debonding stress σ^P is identified as the maximum cohesive

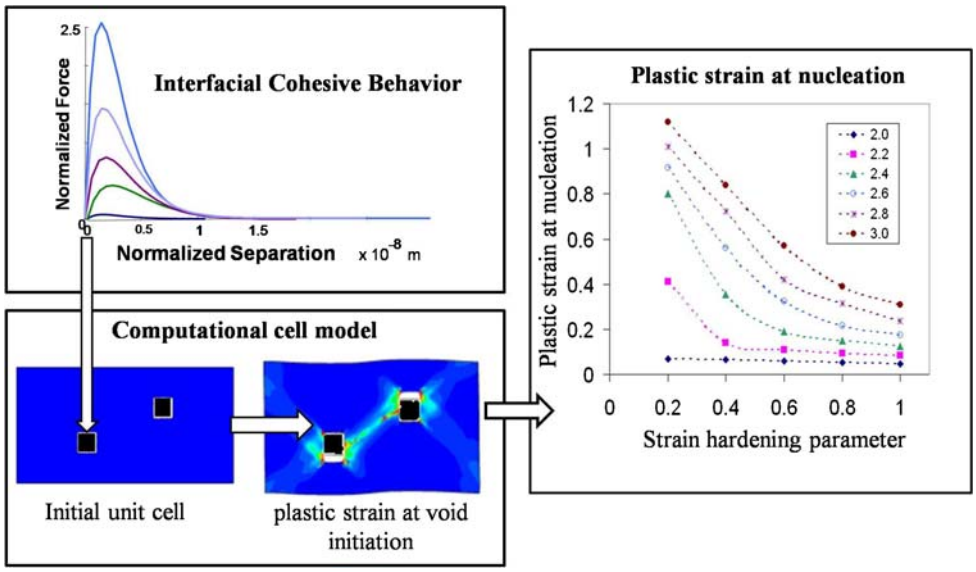

Fig. 4 Nucleation strain as a function of the strain hardening parameter for different debonding peak stress at the Fe–TiN interface

stress. Performing the analysis for different strain hardening parameters h and debonding stress σ^P, a relationship may be derived (as shown in Fig. 4) and used in the constitutive relation described in the previous section. Generally, our simulations show that the nucleation plastic strain decreases with increasing h and increasing σ^P (Fig. 4). This result can be explained by the fact that when the hardening is increased, the stress level at the interface particle/matrix increases at a constant level of average plastic strain. This implies that the harder the matrix material, the earlier the void nucleation.

4 Application to the computation of fracture toughness

In this study, we define the fracture toughness K_{Ic} as the stress intensity factor at which crack growth becomes unstable. This value is determined by plotting the stress intensity factor as a function of the crack opening displacement (COD). The value of K_{Ic} is reached when the slope of the curve changes abruptly as shown in Fig. 5.

4.1 Analysis

The numerical computation of fracture toughness is performed in the context of plane strain, quasi-static conditions. For the assumptions made in Sect. 2 to be ensured, the radius r_K of the circular K-dominant region must be much larger than the radius r of the crack tip. In computations, we use $r_K = 100r$ where $r = 1$ μm is the typical radius of a primary particle. Because the size of primary particles is comparable to the radius of the crack tip, the effect of particle distribution should be accounted for. However, when dealing with a homogenized continuum, the information on particle distribution is lost in the homogenization process. A way to reconcile the two approaches is to have a spatially varying initial volume fraction f^p of primary particles. This can be done by adding a small variation Δf^p to f^p in certain locations that represent the random distribution of primary particles. This method is similar to that introduced by Needleman and Tvergaard [22]. Let us introduce a set of n_p randomly distributed points located at $\{X_1^k, X_2^k\}_{1\le k\le n_p}$ in the reference configuration, with average spacing ℓ_p between primary particles. The primary particle volume fraction f^p is then given as follows:

$$f^p(\mathbf{X}) = \begin{cases} f_0^p + \Delta f^p & \text{when } |\mathbf{X} - \mathbf{X}^k| < R^p \\ f_0^p & \text{when } |\mathbf{X} - \mathbf{X}^k| \ge R^p \end{cases} \tag{16}$$

where R^p is the average radius of a primary particles and $\mathbf{X}$ are the position of material points in the material coordinate system.

4.2 Materials design considerations

We first compare the effective plastic strains around the crack tip given by the conventional continuum model and the multiscale micromorphic continuum model as depicted in Fig. 5. For the conventional model, the classical governing equations of continuum mechanics are solved and the constitutive relation is given by the macroscopic components of that developed for the multiscale model. We note that the small variation of volume fraction shown in (16) was used for both the conventional and multiscale continuum. Figure 5 also shows the comparison between the stress intensity factors K_{Ic}^{cc} and K_{Ic}^{msc} at the onset of crack extension computed with the conventional continuum and the multiscale continuum, respectively.

The conventional continuum solution exhibits the typical spurious localization of the plastic strain in a region deter-

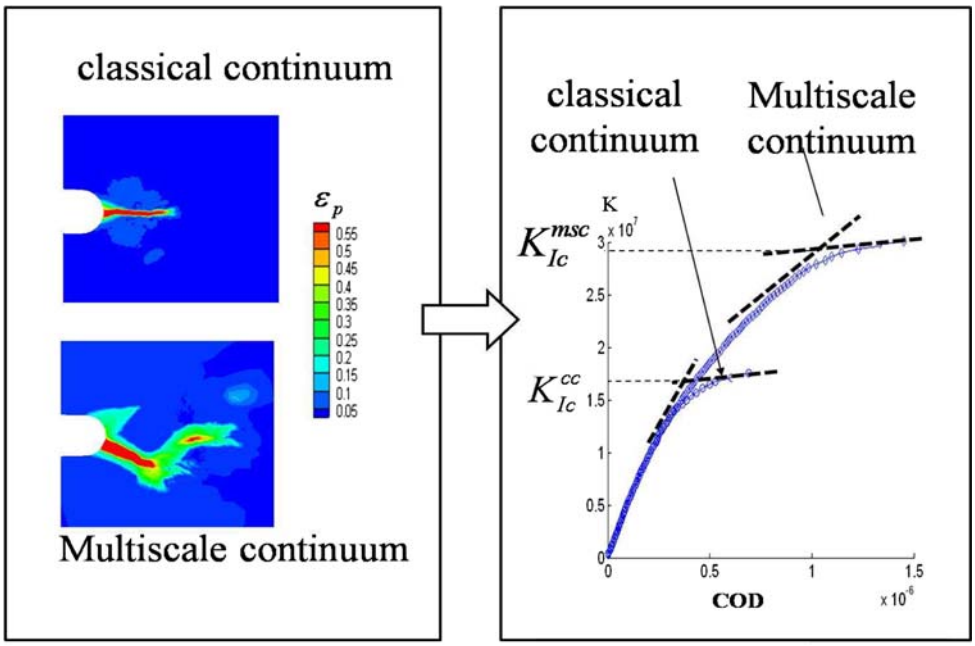

Fig. 5 Comparison of effective plastic strains for the classical (one-scale) continuum and the three-scale continuum

mined by the element size. This non-physical behavior has the effect of underestimating the energy release rate necessary for crack advance and therefore the fracture toughness K_{Ic}^{cc}. On the other hand, with the multiscale technique, the localization region accounts for length scales associated with both primary and secondary particles. Because it accounts for the correct size of the damage region, the multiscale framework allows the dissipation of much more energy into the medium. The energy release rate during crack growth is therefore more important, which leads to higher predicted value of fracture toughness. Note that the lack of symmetry of the strain distribution for the multiscale continuum is due to the spatial variation of initial volume fraction. While this is influencing the solution, the higher fracture toughness is obtained due to the fact that the multiscale model accurately captures the localization lengths and consequently, the correct energy dissipation during crack growth. This last result is more encouraging as the multiscale description is based on the failure mechanisms as explained below.

The evolution of plastic strains at the macro, micro and submicro-scale is depicted in Fig. 6. We can distinguish four stages in the crack growth:

- Development of plastic strains around the crack tip and early nucleation of a void at the sites of primary particles,
- Linking of the crack and void by a shear band whose width is on the order of the size of primary particles (a, b),
- Development of high plastic strain in the shear band until the criterion for void sheet driven coalescence is met. The microscopic shear band (or void sheet) whose size is related to the secondary particles can be observed (c, d, e),
- The last stage is given by micro-void coalescence, giving rise to submicroscopic plastic strain (e). At this stage, the material is fully damaged.

The coupling of mechanisms at different scales is evident from the observation of the tensile stresses σ_{22}, $\overline{\beta}_{22}^{1}$ and $\overline{\beta}_{22}^{2}$ shown in Fig. 7. While the physical meaning of the macrostress σ_{22} is well understood, the existence of the micro and submicrostresses is extremely important in the present analysis since they allow the redistribution of strains during softening and thus are responsible for the correct energy dissipation during fracture. Thus the size of the region for which each stress is observed has to be related to microscopic mechanisms (localization bands between primary and secondary inclusions) presented in Fig. 3. Note that the softening of the macro-stress is associated with the emergence of a micro-stress in the first two sets of figures. Similarly, a softening of the micro-stress (due the presence of the void sheet) leads to the emergence of the submicro-stress.

4.3 Influence of nano-, micro-, and macro-parameters on fracture toughness of HSA

The fracture behavior of HSA is very sensitive to material parameters presents at the nano-, micro- and macro-scale. At the nano-scale, the cohesion between particles and matrix, as well as the properties of the matrix such as the hardening parameter are known to play an important role in the failure of HSA, while at the micro-scale, secondary particle size, volume fraction, and properties dictate the toughness. At the macroscale, parameters relative to primary particles (size, volume fraction, and properties) are the key factors.

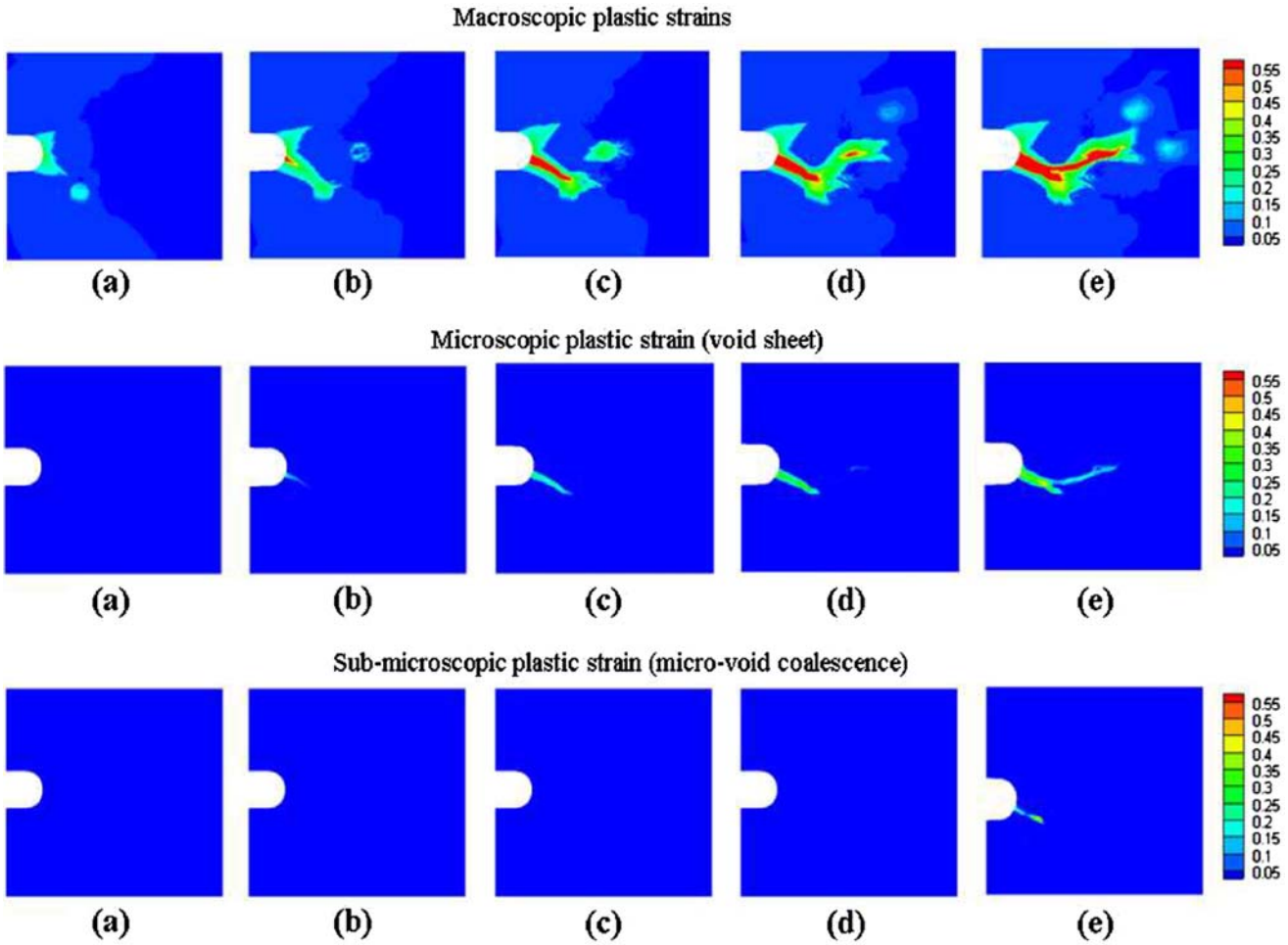

Fig. 6 Evolution of the contours of plastic strains at different scales

The present work aims at providing a relationship between these parameters and the macroscale behavior of HSA during fracture. In particular, the key features of the proposed framework:

- Allows macroscale properties (e.g. strength, hardness, and toughness) and performance to be *predicted* directly in terms of the key statistical described microstructure design parameters including length scales of inhomogeneous deformation,
- Provides a *mathematical link* between microstructure level computational materials design and products design and manufacture.

Since it is based on the continuum theory, one of the strengths of the described multiscale framework is its flexibility in investigating the effect of material parameters on the material's overall mechanical behavior. Moreover, since the material parameters are linked to the microstructure through the computation homogenization described earlier, it is possible to computational quantify how the material response varies when the microstructure changes. This capability opens the door to computational material design for optimal macroscopic properties. As an illustration of how macroscale properties and performance are influenced by key nano/microstructure parameters, trends in fracture toughness are investigated with respect to the variation of four parameters: the debonding stress σ^s at the Fe–TiC interface, the debonding stress σ^p at the Fe–TiN interface, the volume fraction of primary particles f^p, and the hardening parameter h of the matrix material. The fracture toughness K_{Ic} is then written as:

$$K_{Ic} = F\left(h, \sigma^s, \sigma^p, f^p\right) \tag{17}$$

To obtain this function, the fracture toughness calculation presented in Fig. 5 is repeated after varying the material parameters h, σ^s, σ^p and f^p independently, with respect to a microstructure of reference given by material parameters shown in Table 1. The trends in toughness are summarized in Fig. 8.

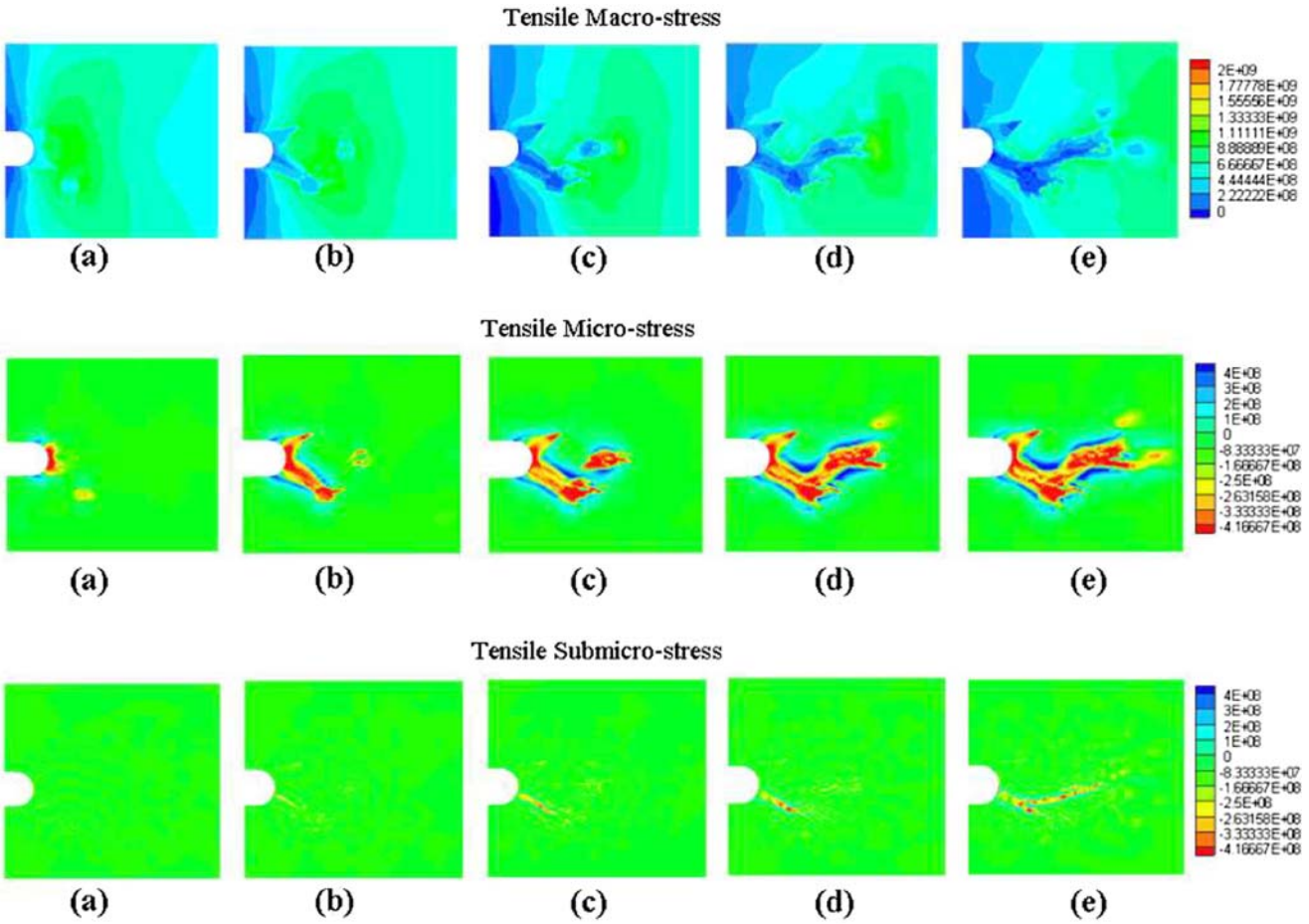

Fig. 7 Evolution of the contours of tensile stress at different scales

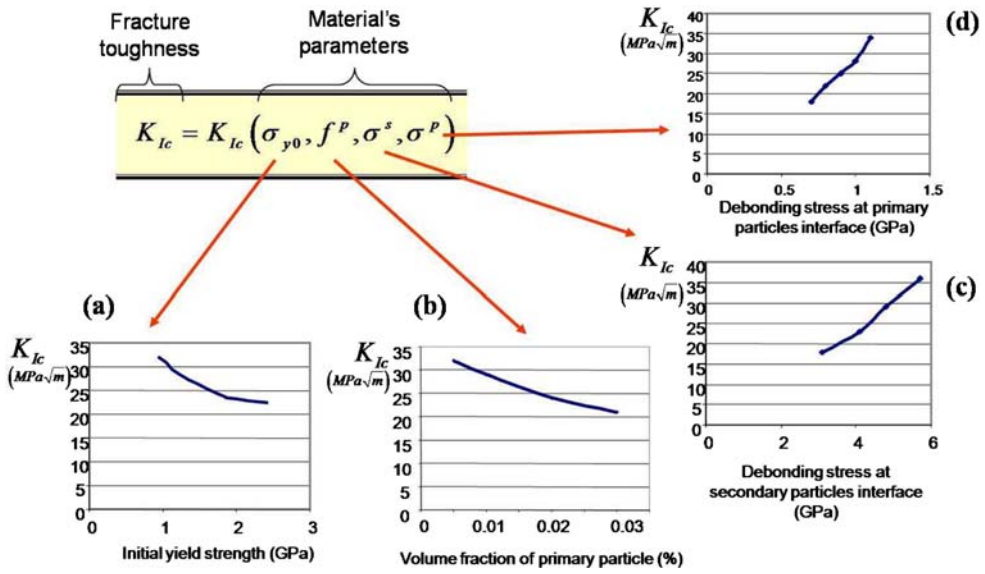

Fig. 8 Variation of fracture toughness as a function of some material key parameters

Figure 8a depicts the variation of fracture toughness with strength, given by the hardening parameter of the matrix material. We observe decreasing fracture toughness with increasing strength that is consistent with experimental observations. This can be explained by the fact that increasing the hardening of the matrix has the effect of precipitating the nucleation of voids by meeting the debonding stress at the particle/matrix interface early in the deformation history. Figure 8d gives the relationship between fracture toughness and debonding peak stress σ^p of the interface Fe–TiN of the primary particles. We observe a very steep increase of fracture toughness with σ^p. The effect of the decohesion stress σ^s at the secondary particle–matrix interface on the fracture toughness is not as significant as the effect of σ^p as shown in Fig. 8c. This trend can be interpreted as follows. After the nucleation of voids from primary particles, stresses and strains become concentrated in the ligament between larger voids. In other words, a small variation in the stress state at the macroscopic level results in a significant variation locally. Consequently, the debonding peak stress σ^s can be reached at a relatively low level of macroscopic stress (or strain) and the influence of the debonding stress is lessened. Figure 8b shows the effect of the volume fraction of primary particles on K_{Ic}. As expected, the fracture toughness increases with decreasing particle volume fraction. This can be explained by the fact that at low volume fraction, voids need to grow independently for a long time before reaching the void sheet driven coalescence criterion.

The main trends can be summarized as follows:

– When strength increases, toughness decreases
– The volume fraction of primary particles and the debonding stress σ^P are critical parameters to the design of fracture toughness, as they are the first initiator of crack growth.
– The debonding stress σ^s is relatively important as large nucleation stress at secondary particles impedes crack growth after nucleation of large voids.

Although it is not the scope of this study, we suggest here that an elaborate parametric study can be performed in detail to understand the relationships between fracture toughness and other macroscopic quantities and the microstructure of HSA. It is thus possible to design the microstructure of HSA by optimizing the microstructure parameter to reach specific material properties.

5 Conclusion

This paper presents a multiscale process zone model that uses concepts from the linear elastic fracture mechanics and the multiscale micromorphic theory. The corresponding multi-length scale finite element formulation is also presented. This approach permits the study of the fracture of hierarchical materials, by considering mechanisms occurring different length scales. In particular, the approach possesses the following features:

- It can be applied to a large class of hierarchical materials and accounts for failure mechanisms and their size effects at each scale of microstructure.
- It is based on a continuum model, which leads to computationally feasible simulations in comparison to brute force models.
- The fracture toughness is a function of the material's key parameters (particles volume fraction, matrix properties, particles/matrix debonding stress, etc.).

The above features make this approach very attractive for computational materials design [15–18]. We have shown that it is possible to perform numerical parametric studies to understand the variation of fracture toughness as a function of various microstructural parameters. The results obtained can then be utilized to optimize the structure of steel to obtain the best combination of strength and toughness.

Acknowledgments The authors gratefully acknowledge the support of the ONR/DARPA D3D Digital Structure Consortium (award N00014-05-C-0241), the National Science Foundation, and the Department of Energy (NSF/Sandia Program).

References

1. Aravas N, McMeeking RM (1985) Microvoid growth and failure in the ligament between a hole and a blunt crack tip. Int J Fract 29:21–38
2. Baaser H, Gross D (2003) Analysis of void growth in a ductile material. Comput Mater Sci 26:28–35
3. Belytschko T, Liu WK, Moran B (2000) Nonlinear finite elements for continua and structures. Wiley, New York
4. Chen JY, Wei Y, Huang Y, Hutchinson JW, Hwang KC (1999) The crack tip fields in strain gradient plasticity: the asymptotic and numerical analyses. Eng Fract Mech 64:625–648
5. Ghosal AK, Narasimhan R (1996) Mixed-mode fracture initiation in a ductile material with a dual population of second-phase particles. Mater Sci Eng A 211:117–127
6. Gurson AL (1977) Continuum theory of ductile rupture by void nucleation and growth. Part 1. Yield criteria and flow rules for porous ductile media. ASME J Eng Mater Technol 99:2–15
7. Hao S, Liu WK, Moran B, Vernerey F, Olson GB (2004) Multiple-scale constitutive model and computational framework for the design of ultra-high strength, high toughness steels. Comput Methods Appl Mech Eng 193:1865
8. Huang Y, Zhang TF, Guo TF, Hwang KC (1997) Mixed mode near-tip fields for cracks in materials with strain gradient effects. J Mech Phys Solids 45:439–465
9. Hutchinson JW (1968) Plastic stress and strain fields at crack tip. J Mech Phys Solids 16(5):337–347
10. Kanninen MF, Popelar CH (1985) Adv Fract Mech. Oxford Engineering Series, Oxford

11. Li S, Liu WK (2004) Meshfree particle methods. Springer, Heidelberg, p 502
12. Liu WK, McVeigh C (2008) Predictive multiscale theory for design of heterogeneous materials. Comput Mech 42(2):147–170
13. Liu WK, Jun S, Zhang YF (1995a) Reproducing kernel particle methods. Int J Numer Methods Fluids 20:1081–1106
14. Liu WK, Jun S, Li S, Adee J, Belytschko T (1995b) Reproducing kernel particle methods for structural dynamics. Int J Numer Methods Eng 38:1655–1679
15. Liu WK, Karpov EG, Zhang S, Park HS (2004) An introduction to computational nanomechanics and materials. Comput Methods Appl Mech Eng 193:1529–1578
16. Liu WK, Karpov EG, Parks HS (2006) Nano mechanics and materials, theory, multiscale, methods and applications. Wiley, New York
17. McVeigh C, Liu WK (2008a) Multiresolution modeling of ductile reinforced brittle composites. J Mech Phys Solids. doi:10.1016/j.jmps.2008.10.015
18. McVeigh C, Liu WK (2008b) Linking microstructure and properties through a predictive multiresolution continuum. Comput Methods Appl Mech Eng 197:3268–3290
19. McVeigh C, Vernerey F, Liu WK, Brinson LC (2006) Multiresolution analysis for material design. Comput Methods Appl Mech Eng 95:37–40, 5053–5076
20. McVeigh C, Vernerey F, Liu WK, Moran B (2007) An interactive microvoid shear localization mechanism in high strength steels. J Mech Phys Solids 55:2, 225–244
21. Needleman A, Tvergaard V (1984) An analysis of ductile rupture in notched bars. J Mech Phys Solids 32:461–490
22. Needleman A, Tvergaard V (1987) An analysis of ductile rupture modes at a crack tip. J Mech Phys Solids 35(2):151–183
23. Needleman A, Tvergaard V (1998) Dynamic crack growth in a nonlocal progressively cavitating solid. Eur J Mech A/Solids 17:421–438
24. Pardoen T, Hutchinson JW (2003) Micromechanics-based model for trends in toughness of ductile metals. Acta Mater 51(1):133–148
25. Rice JR (1967) A path independent integral and the approximate analysis of strain concentration by notches and cracks. Report: E39, 49p
26. Rice JR, Johnson MA (1970) The role of large crack tip geometry changes in plane strain fracture. In: Kanninen MF et al (eds) Inelastic behavior of Solids. McGraw-Hill, New York, pp 641–672
27. Tvergaard V (1988) 3d-analysis of localization failure in a ductile material containing two size-scales of spherical particles. Eng Fract Mech 31:421–436
28. Tvergaard V, Hutchinson JW (1992) The relation between crack growth resistance and fracture process parameters in elastic–plastic solids. J Mech Phys Solids 40:1377
29. Tvergaard V, Hutchinson JW (1996) On the toughness of ductile adhesive joints. J Mech Phys Solids 44:789–800
30. Vernerey FJ, McVeigh C, Liu WK, Moran B, Tewari D, Parks D, Olson G (2006) The 3D computational modeling of shear dominated ductile failure of steel. J Minerals Metals Mater Soc, pp 45–51
31. Vernerey F, Liu WK, Moran B (2007) Multiscale micromorphic theory for hierarchical materials. J Mech Phys Solids 55(12):2603–2651
32. Vernerey F, Liu WK, Moran B, Olson GB (2008) A micromorphic model for the multiple scale failure of heterogeneous materials. J Mech Phys Solids 56(4):1320–1347
33. Xia ZC, Hutchinson W (1996) Crack tip fields in strain gradient plasticity. J Mech Phys Solids 44:1621–1648
34. Xia ZC, Shih CF (1995a) Ductile crack growth—numerical study using computational cells with microstrucurally-based length scales. J Mech Phys Solids 43:233–259
35. Xia ZC, Shih CF (1995b) Ductile crack growth. II. Void nucleation and geometry effects on macroscopic fracture behavior. J Mech Phys Solids 43:1953–1981
36. Xia ZC, Shih CF, Hutchinson W (1994) A computational approach to ductile crack growth under large scale yielding conditions. J Mech Phys Solids 43:389–413
37. Yan C, Mai YW (1998) Effect of constraint on void growth near a blunt crack tip. Int J Fract 92:287–304